MATERIALS SCIENCE

Rational synthesis of an atomically precise carboncone under mild conditions

Zheng-Zhong Zhu[1]*, Zuo-Chang Chen[1]*, Yang-Rong Yao[1], Cun-Hao Cui[1], Shu-Hui Li[1], Xin-Jing Zhao[1], Qianyan Zhang[1†], Han-Rui Tian[1], Piao-Yang Xu[1], Fang-Fang Xie[1], Xiao-Ming Xie[1], Yuan-Zhi Tan[1], Shun-Liu Deng[1], Jennifer M. Quimby[2], Lawrence T. Scott[2,3], Su-Yuan Xie[1†], Rong-Bin Huang[1], Lan-Sun Zheng[1]

Carboncones, a special family of all-carbon allotropes, are predicted to have unique properties that distinguish them from fullerenes, carbon nanotubes, and graphenes. Owing to the absence of methods to synthesize atomically well-defined carboncones, however, experimental insight into the nature of pure carboncones has been inaccessible. Herein, we describe a facile synthesis of an atomically well-defined carboncone[1,2] ($C_{70}H_{20}$) and its soluble penta-mesityl derivative. Identified by x-ray crystallography, the carbon skeleton is a carboncone with the largest possible apex angle. Much of the structural strain is overcome in the final step of converting the bowl-shaped precursor into the rigid carboncone under mild reaction conditions. This work provides a research opportunity for investigations of atomically precise single-layered carboncones having even higher cone walls and/or smaller apex angles.

INTRODUCTION

As new structural forms of carbon, carboncones were first observed as structural defects on the endcaps of deformed carbon nanotubes (CNTs) by Iijima and co-workers in 1992 (*1*). A series of carboncones with one, two, three, four, or five pentagons on the cone cap were subsequently observed by electron microscopy (Fig. 1A) (*2*, *3*). Carboncones can be considered as intermediate species along the continuous formal transition (*2*) from fullerenes to graphenes through a tubular-like stage, resembling a zero-dimensional (0D) cluster at the apex, then proceeding to a 1D tube, and, finally, approaching a 2D graphene. Largely owing to their unique conical shapes and hollow structures, carboncones hold particular promise for applications such as scanning probe tips (*4*), electron field emitters (*5*), and gas storage materials (*6*). Some chemical-physical techniques, including chemical vapor deposition (*4*), laser ablation (*7*), arc discharge (*1*), and pyrolysis of organic compounds (*3*), have been developed to produce multilayered carboncones, but yields of those carboncones are rather low. Moreover, mixtures of carboncones with varying cone angles and heights were typically produced together with impurities of carbon discs and CNTs in carbon soots (*3*). It remains challenging to get rid of the impurities from these mixtures and to synthesize a single-layered carboncone. Research of carboncones has been severely hampered by the limitations of the previous synthetic technology in the past 20 years. Consequently, insight into the nature of well-defined single-layered carboncones has been inaccessible, and controllable methods for synthesizing structurally uniform carboncones are strongly desired.

Herein, we reported a bottom-up organic chemical approach to prepare a carboncone molecule **1a** ($C_{70}H_{20}$) and its penta-mesityl derivative **1b** under mild reaction conditions. The carboncone framework of the newly synthesized molecules with a single pentagonal cone cap and a hexagonal lattice cone wall has been unambiguously identified by x-ray crystallography (Fig. 1B).

To better communicate about carboncones with varying cone caps and cone walls, we proposed a nomenclature of carboncone[*n*,*m*]. Here, "*n*" refers to the number of pentagons on the cone cap ("*n*" determines the apex angle of the cone), and "*m*" refers to the number of intact circles consisting of fused pentagonal/hexagonal rings ("*m*" determines the height of the cone in some senses). Shown in Fig. 1A are a series of typical carboncone[*n*,*m*] in which *n* = 1 to 5 and *m* = 3 or 4. The newly synthesized carboncone skeleton can be defined as a carboncone[1,2], in which the "1" indicates one pentagon on the cone cap and the "2" reflects two intact circles of fused hexagonal rings between the cone tip and the cone rim (Fig. 1A). Note that the nomenclature of carboncone[*n*,*m*] does not exclude structures having irregular or incomplete rims. Strictly speaking, for example, the skeleton of carboncone **1** is a pentanaphtho-carboncone[1,2]. Similar inclusiveness is likewise found in the definition for CNT [*n*,*m*] (*8*). As outlined in Fig. 1, the tip of the carboncone can be a point in the center of a pentagonal/hexagonal ring or a point at the middle of the central carbon-carbon bond. According to this definition, the well-known corannulene molecule can be defined as a "cone cap," including only a single circle of fused hexagonal rings around the cone tip, rather than as a carboncone, which must have at least one circle of cone wall in addition to a cone cap. Notably, the carboncone with five pentagons on the cone cap, such as carboncone[5,4], have no centrosymmetric point; as a result, the carboncone wall between the cone tip and the cone rim is uneven, and the carboncone[5,4] looks tilted.

RESULTS

Synthesis and structures of carboncone[1,2] derivatives 1

As shown in Fig. 2, the carboncone[1,2] derivatives **1a** and **1b** were synthesized by three-step organic chemical processes starting from corannulene **2**. Direct borylation of **2** with $B_2(pin)_2$ afforded

[1]State Key Lab for Physical Chemistry of Solid Surfaces, Collaborative Innovation Center of Chemistry for Energy Materials, Department of Chemistry, College of Chemistry and Chemical Engineering, Xiamen University, Xiamen 361005, China. [2]Merkert Chemistry Center, Boston College, Chestnut Hill, MA 02467-3860, USA. [3]Department of Chemistry (0216), University of Nevada, Reno, 1664 N. Virginia St., Reno, NV 89557, USA.
*These authors contributed equally to this work.
†Corresponding author. Email: xmuzhangqy@xmu.edu.cn (Q.Z.); syxie@xmu.edu.cn (S.-Y.X.)
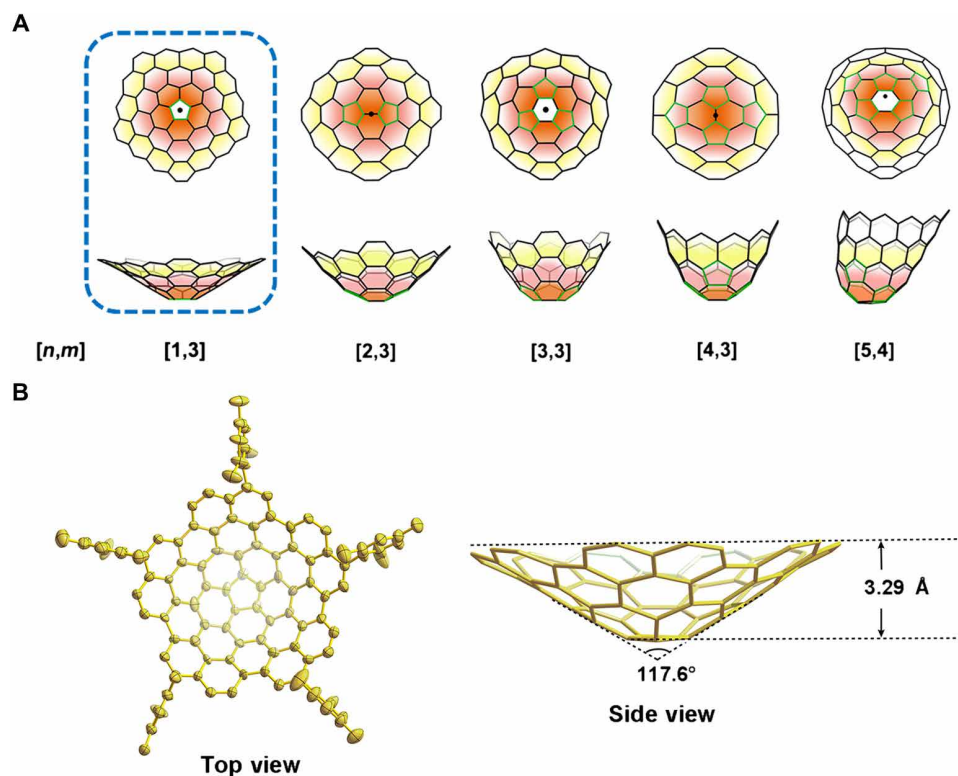
Fig. 1. Structures of carboncone. (**A**) Illustration of all five types of carboncone[*n,m*] (*n* = 1 to 5, *m* = 3 and 4). The bonds of pentagon are marked with green lines. The circles of fused rings are painted with orange, pink, yellow, and white from tips to rims, respectively. The black dot points to the cone tip. (**B**) The Oak Ridge thermal-ellipsoid plot (ORTEP) diagram of the penta-mesityl carboncone[1,2] derivative (**1b**) at 50% probability with hydrogen atoms and solvent molecules omitted for clarity (top view), and stick model diagram of crystallographic structure of **1b** with five mesityl groups, hydrogen atoms, and solvent molecules omitted for clarity (side view). The cone height and the apex angle in the crystal are displayed.

1,3,5,7,9-pentakis(Bpin)corannulene **3** (*9*) as the major product. Then, fivefold Suzuki-Miyaura coupling of **3** with 1-bromonaphthalene **4a** or 1-bromo-4-mesitylnaphthalene **4b** gave *sym*-penta(1-naphthyl) corannulene **5a** or *sym*-penta(4-mesityl-1-naphthyl)corannulene **5b** in moderate yields (figs. S1 to S6). Last, when cyclodehydrogenation reaction conditions were applied to the bowl-shaped polycyclic aromatic hydrocarbons (PAHs) **5** (*10*), completely closed products **1** were obtained by stitching together the five appendages of **5**.

The hydrogen-terminated carboncone[1,2] **1a** is rather poorly soluble in common organic solvents, likely owing to the strong van der Waals attractions associated with large-area intermolecular contacts between curved faces. Owing to such a low solubility, carboncone **1a** was characterized only by high-resolution mass spectrometry with matrix-assisted laser desorption ionization (MALDI) (fig. S7), which confirmed the molecular formula of **1a** as $C_{70}H_{20}$. In addition to the major component of the completely closed **1a**, a mixture of some unidentified products likely arising from incomplete closure were also detected in the mass spectra (fig. S7). To improve the solubility of **1a**, we introduced mesityl groups at the 4-postion of the naphthyl units. As anticipated, the corresponding ring closure product **1b** was synthesized in moderate yield and exhibited much improved solubility compared with **1a**.

With sufficient solubility in common organic solvents (e.g., dichloromethane, carbon disulfide, and toluene), the carboncone[1,2] derivative **1b** can be characterized by routine techniques, such as nuclear magnetic resonance (NMR) spectroscopy and mass spec-

trometry (figs. S8 to S11). The ^1H NMR spectrum of **1b** reveals the presence of five different types of aromatic protons (three singlets and two doublets) (fig. S9), indicating that **1b** has C_5 symmetry. The calculated ^1H NMR spectrum of carboncone **1b** is in good agreement with the experimentally observed spectrum (fig. S10). As expected, in the aromatic region, the ^{13}C NMR spectrum shows 20 signals: 138.80, 138.71, 137.84, 137.47, 137.28, 136.97, 130.05, 129.02, 128.93, 128.65, 127.98, 127.91, 125.18, 125.08, 124.73, 124.68, 124.57, 123.72, 123.66, and 123.53 ppm (fig. S11).

A single crystal of **1b** suitable for x-ray analysis was obtained by slow diffusion of hexane into a carbon disulfide solution of **1b** (table S1). In accordance with NMR spectra (figs. S9 to S11), the crystallographic structure of **1b** confirms carboncone[1,2] having a C_5 symmetrically conical shape with one pentagon embedded in 25 hexagons (Fig. 1B). The unique conical curvature of carboncone[1,2] distinguishes it from the dozens of known buckybowls (*11*) and fullerenes (*12*) that also exhibit positive geodesic curvature.

In the parent carboncone[1,2] of **1b**, 70 sp^2-carbon atoms are completely conjugated. The experimentally determined apex angle of **1b** is 117.6° (Fig. 1B), which is slightly larger than that of the large cone shown in the topological model (112.9°) (*1, 2*). The central corannulene moiety adopts a cone-shaped geometry with a depth of 1.16 Å, which is substantially deeper than that of the parent corannulene (0.86 Å). The cone height, defined as the distance between the center of the pentagon and the mean plane of the 10 furthest rim carbons, is 3.29 Å (Fig. 1B). The p-orbital axis vector (POAV) angle of the
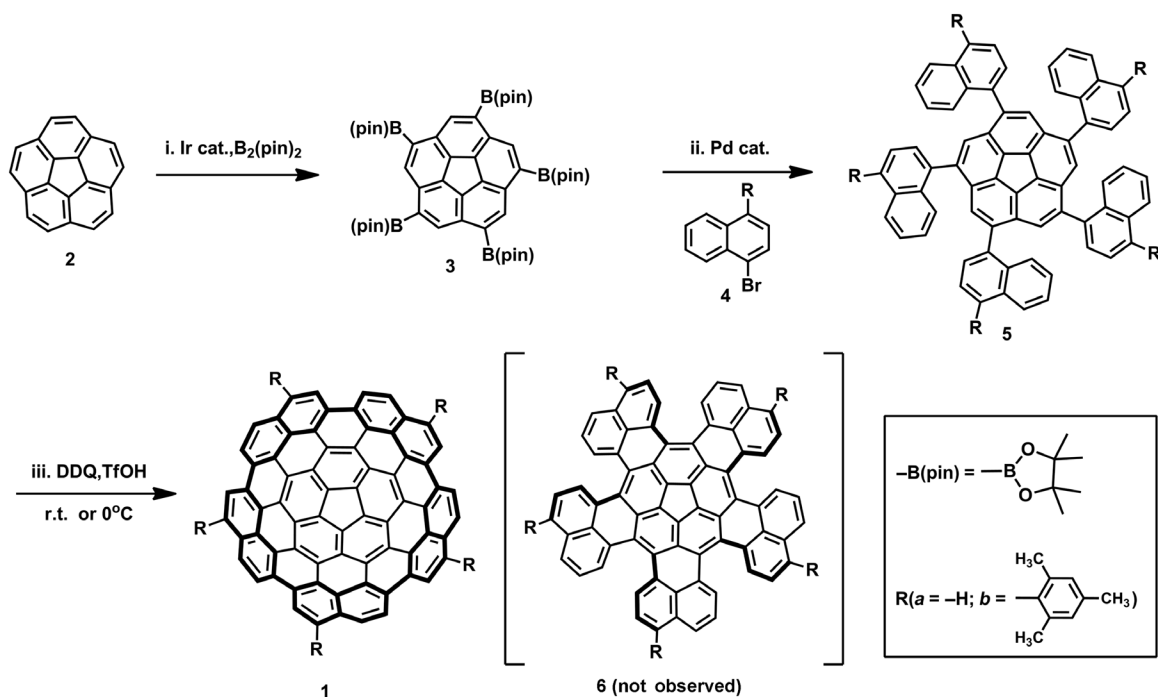
Fig. 2. Three-step organic synthesis of the carboncone[1,2] derivatives 1 from corannulene 2. Conditions: (i.) (Ir(OMe)cod)$_2$ [20 mole percent (mol %)], B$_2$(pin)$_2$ (6.5 equiv.), 4,4'-dimetylpyridine (40 mol %), sodium methoxide (10 mol %), cyclohexane, 85°C, 4 days; (ii.) 1-bromonaphthalene or 1-bromo-4-mesitylnaphthalene (10 equiv.), Pd(PPh$_3$)$_4$ (25 mol %), Cs$_2$CO$_3$ (30 equiv.), toluene/H$_2$O (2:1), 100°C, 24 hours; (iii.) DDQ (20 equiv.), TfOH/CH$_2$Cl$_2$ (1:20), 10 min. cod, 1,5-cyclooctadiene; pin, pinacolato; cat., catalyst; DDQ, 2,3-dichloro-5,6-dicyano-1,4-benzoquinone.

carbon atoms in the cone tip of **1b** (10.5°) is also larger than that in the parent corannulene (8.2°) (*13*) but smaller than that in the fullerene C$_{60}$ (11.6°) (*13*). The steric hindrance provided by the five mesityl groups in **1b** prevents the molecules from stacking in a concave-to-convex orientation (*14*). Rather than forming a columnar arrangement in the crystal, a staggered packing is adopted (fig. S12). In addition, the cone-to-cone inversion energy of **1a** and **1b** (166.4 and 167.0 kcal/mol, respectively) through an S-shaped transition state was estimated by density function theory (DFT) calculations, and is 188.8 kcal/mol for **1a** if through a hypothetical flat transition state structure (see figs. S13 and S14, table S2, and Computational methods in Materials and Methods). These large inversion energies exceed the bond dissociation energies of even the strongest Csp^2—Csp^2 bonds and indicate that the geometric structure of carboncone[1,2] must be quite rigid.

Theoretical understanding of the ring closure reaction from the precursor 5 toward 1

Theoretical calculations were performed to understand the final ring closure reaction. The strain energy of **1b** (98.4 kcal/mol) and the strain increase in the final closure step (43.5 kcal/mol) were estimated by DFT calculations (see fig. S15 and Computational methods in Materials and Methods).

To understand why the ring closure from the precursor **5** toward **1** can be completed under these mild reaction conditions, we proposed a rational Scholl ring closure reaction pathway leading to carboncone[1,2] (**1a**) with the lowest barriers in each step of cyclization (Fig. 3). For the most likely pathway shown in Fig. 3 (blue and red hexagons closing alternately but not always adjacent), the activation energies associated with the formation of the red hexagons

appear to be lower than those for the formation of the blue hexagons. To probe the differences between the red and the blue hexagons, we calculated nucleus-independent chemical shifts (NICS) (*15*) for the new rings in each of the assumed intermediates (Fig. 3). The calculation results show that the NICS values of the red rings range from −6.28 to −9.94, indicating a strong aromatic character. The blue hexagons, on the other hand, are revealed to be nonaromatic, with NICS values ranging from +2.38 to +6.98. These differences in value of NICS suggest that formation of the aromatic red hexagons makes favorable contributions to reduce barriers of the steps of cyclization.

Energy barriers for each step of cyclization were calculated by a dication pathway (*16*) in the polarized continuum model with dichloromethane solvent (figs. S16 to S23). All possible modes of six-membered ring formation in 10 total cyclizations were considered, and the corresponding energy barriers were obtained (shown in figs. S16 to S22). Taking the calculations of ring formation on **A2** as an example, the formation of an adjacent aromatic hexagon ($\Delta E^{\neq}_{2–1} = 11.6$ kcal mol^{-1}) is much easier than the formation of the other nonaromatic hexagons (from **A2** to **A2-2**, **A2-3**, **A2-4**, or **A2-5**) (fig. S16). Note that the pathway of the first formation of all five nonaromatic blue hexagons (rather than the five aromatic red hexagons) looks less likely because the cyclization of the three nonaromatic blue hexagons must overcome very high barriers, as shown in fig. S23, which might explain why the hypothetical intermediate **6** in Fig. 2 was not observed in the mixture of ring closure products.

Spectrometric and electrochemical properties of 1b

1b was dissolved in CH$_2$Cl$_2$ to give an orange solution with two intense absorptions around 287 and 456 nm, as well as some weaker
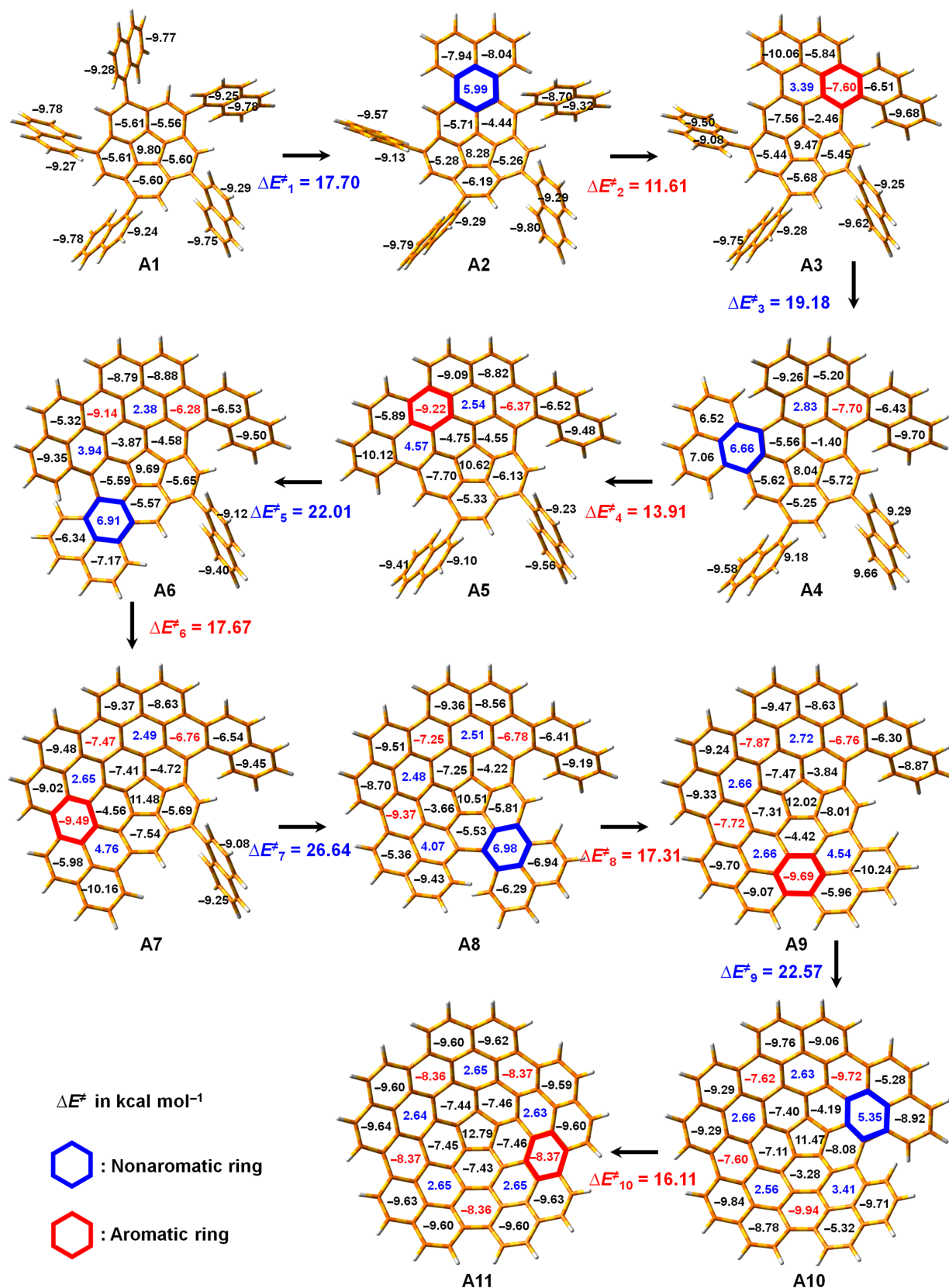
Fig. 3. A rational ring closure pathway from the precursor 5a toward 1a calculated by a dication pathway. Here, $\Delta E^{\ddagger}$ represents the energy barrier for each step of cyclization. The NICS values of the rings in all intermediate products from **A1** to **A11** are presented.

peaks. The longest wavelength absorption maximum appears at 526 nm, with a tail in the visible region that extends beyond 600 nm (Fig. 4A). Time-dependent (TD)–DFT calculations at the B3LYP/6-31G(d,p) level reveal that the transition energies and oscillator strengths show good agreement with the observed ultraviolet-visible (UV-vis) absorption values of **1b** (Fig. 4A). The attributions of major absorption bands at 292, 350, and 455 nm are listed in table S3. For comparison, spectra of both grossly warped nanographene (**7**; $C_{80}H_{30}$, with one pentagon and five heptagon defects; fig. S15) (*17*) and planar nanographene (**8**; $C_{78}H_{30}$, defect free; fig. S15) (*18*) are shown in fig. S24. The experimental absorption data confirm the DFT predictions that both **1a** and **1b** have slightly narrower bandgaps than those of **7** and **8** ($E_{HOMO} = -5.18, -5.10, -5.12,$ and -4.96 eV; $E_{LUMO} = -2.30, -2.25, -2.10,$ and -2.05 eV for **1a**, **1b**, **7**, and **8**, respectively) (HOMO indicates highest occupied molecular orbital; LUMO, lowest unoccupied molecular orbital) (figs. S25 to 27 and table S2). The emission of **1b** was measured at ambient temperature with excitation at 456 nm, and fluorescence maxima were observed at ~565 and 604 nm with several additional shoulders (the measured quantum efficiency is about 3.3%) (Fig. 4A). The infrared (IR) absorption spectrum of **1b** measured in the solid state, shown in Fig. 4B, covers the range from 450 to 3350 cm^{-1}. It is dominated by

three bands and two humps, labeled with asterisks, at 1120.5, 1384.7, 1629.6, 2850.4, and 2919.8 cm^{-1}. A calculated spectrum is displayed in the same figure for comparison, and calculated positions of the most prominent bands are given in table S4.

Besides the spectrometric characterizations, the electrochemical properties of **1b** were studied by cyclic voltammetry (Fig. 4, C and D). For comparison, the cyclic voltammogram of corannulene **2** was measured under the same conditions. The electrochemical data reveal that **1b** has a much higher reduction voltage relative to that of **2** (Fig. 4C).

DISCUSSION

Synthesis of carboncone[1,2] under mild conditions

It is remarkable that the carboncone[1,2] derivatives **1** can be synthesized in just three simple steps, starting from commercially available corannulene **2**. In particular, in the final organic chemical reaction that produces carboncone, the oxidative cyclizations do not stop at the fivefold annulated product pentaphenalenocorannulene **6**, but they continue all the way to a completely closed product **1** by stitching together the five appendages of **5** (Fig. 2). The 10 new Csp²—Csp² bonds are formed effectively to overcome the structural
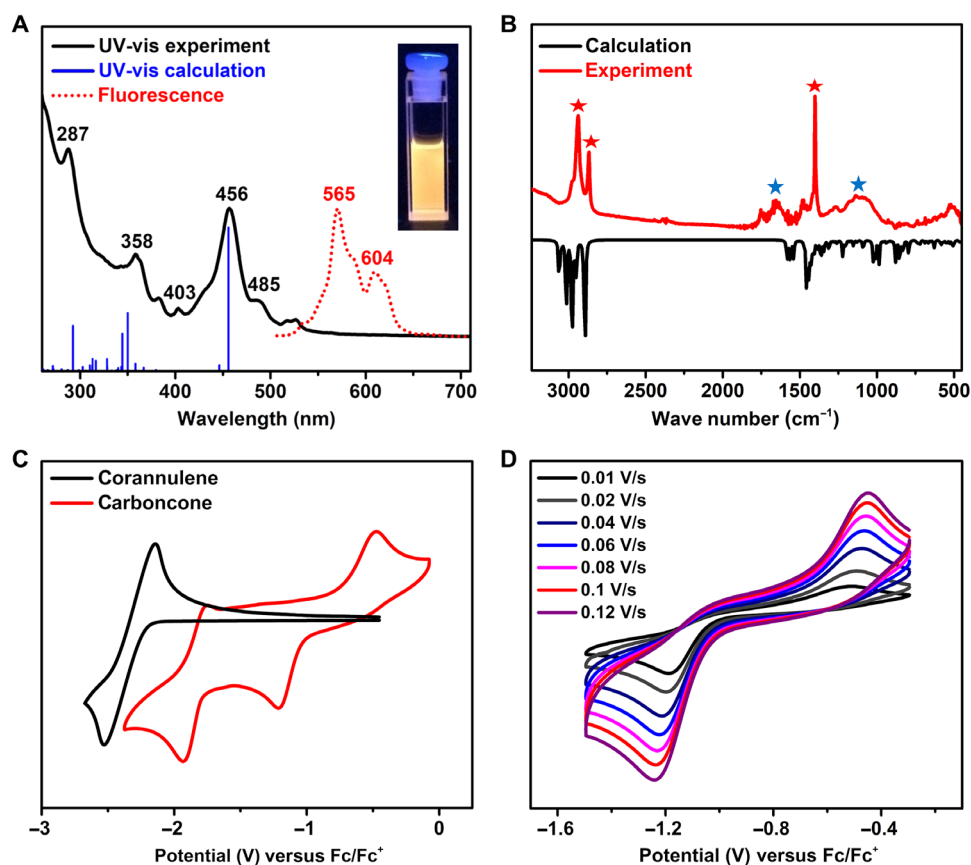

Fig. 4. Spectrometric and electrochemical properties of the penta-mesityl carboncone[1,2] derivative (1b). (**A**) Ultraviolet-visible (UV-vis) absorption (black solid line), the oscillator strengths (blue bars) obtained by TD-DFT calculations at the B3LYP/6-31G(d,p) level of theory, and emission spectra (red dashed line) of **1b** in CH₂Cl₂. Inset: Digital photograph of a CH₂Cl₂ solution of **1b** irradiated at 456 nm. (**B**) IR absorption spectrum of **1b**. Asterisks mark the dominant bands and humps at 1120.5, 1384.7, 1637.3, 2850.4, and 2919.8 cm⁻¹ in the observed spectrum (red). A theoretical spectrum (black) calculated at the B3LYP/6-31G(d,p) level of theory is shown for comparison. (**C**) Cyclic voltammogram of **1b** and corannulene in *N,N*-dimethylformamide. (**D**) The first redox process of **1b** measured in *o*-dichlorobenzene at variable scan rates (120, 100, 80, 60, 40, 20, and 10 mV/s).
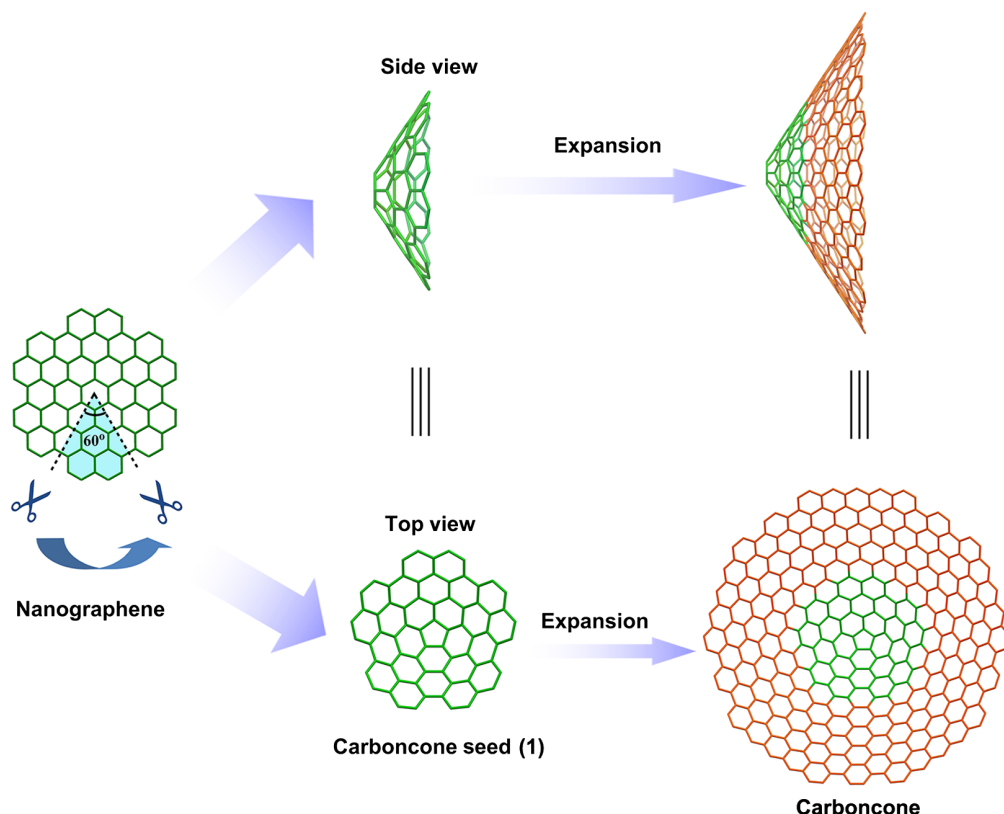
Fig. 5. Topology structure and strategy for the bottom-up synthesis of structurally uniform carboncones[1,m]. Carboncone[1,2] molecule (**1**) is formed by introducing a 60° positive disclination defect in the nanographene sheet, and the growth of carboncone[1,m > 2] undergoes epitaxial expansion from the carboncone[1,2] seed molecule (**1**).

strain in the final closure step, which is quite mild, occurring even at 0°C. By contrast, the syntheses of buckybowls (*11*, *13–14*, *19–20*) with curvatures similar to carboncone[1,2] required much more severe reaction conditions, such as 180°C in solution or temperatures around 1000°C in the gas phase.

Within the toolbox of methods for critical constructions of Csp^2—Csp^2 bonds in strained hydrocarbon compounds, flash vacuum pyrolysis (FVP) (*11*) and metal-catalyzed intramolecular ring-closing arylations (*19–20*) have been the two main strategies. Other strategies include reductive coupling followed by oxidation with DDQ (2,3-dichloro-5,6-dicyano-1,4-benzoquinone) (*21*) and C—F activation with silyl cation reported by Siegel and co-workers (*22*), McMurry coupling reported by Sygula and Rabideau (*23*), and alumina-promoted cove-region closure by elimination of hydrogen fluoride (HF) reported by Amsharov *et al.* (*24*). Recently, the venerable Scholl reaction, which has been pushed to spectacular heights by Müllen and co-workers (*18*) for the synthesis of many strain-free planar nanographenes in the last 10 to 15 years, was used by Itami and co-workers (*17*) to synthesize grossly warped nanographenes (*7*; fig. S15). In contrast to those warped nanographenes (*17*, *25*), which embody negative curvature owing to the presence of five heptagons in their structure, the present new carboncone[1,2] displays only positive curvature resulting from one pentagonal defect in the hexagonal lattice. To the best of our knowledge, the Scholl reaction has never been used before as a ring closure strategy to synthesize a buckybowl having positive curvature.

Electronic properties of the carboncone[1,2]
DFT calculations at the B3LYP/6-31G(d,p) level reveal that the LUMO of carboncone[1,2] (**1**) is lower lying than that of the parent corannulene **2** (figs. S25 and S26 and table S2), which is in agreement with the cyclic voltammetric data (Fig. 4C) with the much higher reduction voltage of **1b** relative to that of **2**. Likely carboncones with higher cone walls should have higher reduction voltages, corresponding to lower LUMO levels and stronger electron-accepting abilities. In addition, the scan rate–dependent potential difference of **1b** (Fig. 4D) indicates a quasi-reversibility of the first redox process of **1b**. It is likely that the remaining electrons are left on the pentagon of carboncone **1b**, making it relatively harder to lose than the normal electron on the carboncone.

Bottom-up growth of carboncone[1,m] with carboncone[1,2] as seed
Benefiting from the bottom-up chemical synthesis strategies, some structurally well-defined carbon nanostructures, such as cyclopara-phenylenes (*26*), the shortest CNT endcap (*27*), and carbon nano-belts (*28*), have been synthesized and sought as seeds for controlled syntheses of single-walled CNT (SWCNT) materials. A number of attempts to grow single-index SWCNTs from the well-defined seed molecules by analogous processes have already been reported (*29–34*). The carbon skeleton of **1**, with a single pentagon-containing cone cap encircled by a lattice of fused hexagons, corresponds to a 60° positive disclination defect introduced into a graphene network (Fig. 5)

(1, 2). By the same token, this carboncone[1,2] molecule is very promising as a seed from which to grow structurally uniform carboncones by repetitive addition of carbon atoms to annulate new hexagonal rings (Fig. 5). All the expanded carboncones would have the same apex angles in the family of carboncone[1,m].

CONCLUSIONS

In summary, the first carboncone[1,2] molecule **1a** ($C_{70}H_{20}$) and its penta-mesityl derivative **1b** have been effectively synthesized starting from corannulene $C_{20}H_{10}$ in just three steps using mild organic chemical reactions. The reaction mechanism for the feasible Scholl reaction in the critical ring closure process leading to the strained carboncone[1,2] molecule has been explained theoretically. The unique structure of the penta-mesityl carboncone **1b** caused by one pentagon in the hexagonal lattice of trigonal carbon atoms was confirmed by single-crystal x-ray crystallography. DFT calculations reveal that the cone-shaped carboncone[1,2] is rigid and protected from cone-to-cone inversion by an exceptionally high energy barrier. The UV-vis and IR absorptions of **1b** are shown to be comparable with those of sp^2-hybridized planar and warped nanographene with similar size, whereas the electrochemical properties differentiate it from its parent corannulene. Carboncone[1,2] not only provides valuable clues into how other carboncone[n,m] might be prepared but also gives a very promising seed from which to controllably grow uniform carboncone[1,m] materials and a possibly suitable species for the study of carbon-rich molecules similar to fullerenes and PAHs in interstellar space.

MATERIALS AND METHODS

Materials

Unless otherwise noted, all materials including dry solvents were obtained from commercial suppliers and used without further purification. Unless otherwise noted, all reactions were performed with dry solvents under an atmosphere of argon in dried glassware with standard vacuum-line techniques. All workup and purification procedures were carried out with reagent-grade solvents in air. Analytical thin-layer chromatography (TLC) was performed using E. Merck silica gel 60 F254–precoated plates (0.25 mm). Corannulene **2** was synthesized according to the reported procedure (35).

NMR spectroscopy

^1H NMR (400, 500, and 600 MHz) and ^{13}C NMR (100, 150, and 210 MHz) spectra were recorded using a Bruker AV 400 (600 or 850) spectrometer at 298 or 323 K. Chemical shifts were reported on the delta scale in parts per million relative to $CHCl_3$ ($\delta = 7.26$ ppm), CH_2Cl_2 ($\delta = 5.32$ ppm), and $C_2H_2Cl_4$ ($\delta = 6.00$ ppm) for ^1H NMR, and $CDCl_3$ ($\delta = 77.0$ ppm) and CD_2Cl_2 ($\delta = 55.0$ ppm) for ^{13}C NMR. The ^1H NMR spectra data were presented as follows: chemical shift, multiplicity (s, singlet; d, double; and m, multiplet), and integration.

Mass spectrometry

High-resolution mass spectra (HRMS) were determined on a Bruker Daltonics Ultraflex III Time-of-Flight (TOF)/TOF (MALDI-TOF MS) or on a JEOL JMS-S3000 Spiral TOF (MALDI-TOF MS).

IR spectroscopy

The IR spectra were obtained using a Thermo Scientific Nicolet 380 IR spectrometer.

UV-vis absorption and fluorescence emission spectroscopy

UV-vis absorption spectra were recorded on a Shimadzu UV-2550 spectrometer with a resolution of 0.5 nm. Emission spectra were recorded on an Edinburgh fls980 spectrometer with a resolution of 0.4 nm and automatically corrected by instrumental function. Dilute solutions in degassed spectral grade dichloromethane in a 1-cm square quartz cell were used for measurements. Absolute fluorescence quantum yields were determined with a Hamamatsu C9920-02 calibrated integrating sphere system equipped with a multichannel spectrometer (PMA-11).

Cyclic voltammetry

Cyclic voltammetry was performed on an Als/600D electrochemical analyzer. The cyclic voltammetric cell consisted of a Pt electrode, a Pt wire counter electrode, and an $Ag/AgNO_3$ reference electrode. The measurements were carried out at a scan rate of 100 mV/s or a variable of 10 to 120 mV/s with tetrabutylammonium hexafluorophosphate ($^nBu_4NPF_6$) as the supporting electrolyte.

X-ray diffraction

X-ray crystallographic data of compound **1b** were collected on a Rigaku x-ray single crystal diffractometer (XtaLAB PRO MM007-DW) using a rotating-anode x-ray as the diffraction source with Cu Kα radiation ($\lambda = 1.54184$ Å) at 100 K. The structure was solved by intrinsic phasing with the program of SHELXT-2014 (36), and all non-hydrogen atoms were refined anisotropically by the full-matrix least-squares method on F^2 with the program of SHELXL-2018 (36) within the program of Olex2 (37). The refined structure shows a slight disorder. The minor part of the central C_{70} with an occupancy of 0.328 was regulated using 46 restraints, whereas the major part with an occupancy of 0.672 was completely free of restraints with unambiguous geometric configuration and reasonable atomic temperature factors (the equivalent isotropic atomic displacement parameters U_{eq} ranging from 0.046 to 0.068 $Å^2$). The obtained crystallographic data support that the structure had relatively separated electron density centers for each of the two disordered parts (with one-third and two-third occupancy, respectively), and the disorder had negligible influence to the determination of the structure in the major part with two-third occupancy.

Computational methods

DFT calculations were performed on the Gaussian 09 program (38) using the B3LYP method and 6-31G(d,p) basis set. The Cartesian coordinates and energies of all optimized species are shown in table S2. All transition states were obtained with one imaginary frequency and checked by intrinsic reaction coordinate (IRC) calculations. The mesityl groups were replaced by hydrogen atoms to reduce the workload of computation in the calculations of transition states in the dication pathway. The hexa-(4-mesityl-naphthyl)-coronene (**9b**) and its ring closure compound (**10b**) can be taken as the strain-free references (fig. S15) in the related strain energy calculations of **1b** and **5b**. The strain energies (ΔG) of **1b** and **5b** were estimated by comparing the electronic and thermal free energies (G) of **1b** and **5b** to 5/6 of the corresponding strain-free reference compound **10b** and **9b**, respectively. In the calculation of cone-to-cone inversion energies, the S-shaped transition state structures of **1a** and **1b** are analogous to the transition state of the bowl-shaped fragment of C_{70} reported by Wu et al. (39) (shown in fig. S13 and table S2). In addition, the C—C bonds of the outer rings in the flat structure of **1a** suffer so much stretching force that

it will squeeze the flat structure into an S-shaped structure in the transition state calculation. To solve this dilemma, all carbon atoms were restricted in the same plane in the optimization of the flat structure for the transition state of **1a**.

Synthesis of 4-mesitylnaphthalen-1-amine (S2)

To a solution of $Pd(OAc)_2$ (112 mg, 0.5 mmol, and 5 mole percent (mol%)], SPhos (40) (400 mg, 1 mmol, and 0.1 equiv.), 4-bromonaphthalen-1-amine (**S1**, 2.21 g, 10 mmol, and 1.0 equiv.), and mesitylboronic acid (1.8 g, 11 mmol, and 1.1 equiv.) in toluene (100 ml) was added a solution of K_3PO_4 (6.36 g, 30 mmol, and 3.0 equiv.) in H_2O (10 ml), and the resultant mixture was stirred at 100°C for 6 hours under nitrogen. After cooling the mixture to room temperature, the reaction mixture was extracted with CH_2Cl_2. The combined organic layers were dried over Na_2SO_4, and the solvent was removed under reduced pressure. The crude product was purified by silica gel column chromatography (eluent: hexane/CH_2Cl_2 = 1:2) to give 4-mesitylnaphthalen-1-amine (**S2**, 2.35 g, 90%) as a purple solid. ^1H NMR (400 MHz, $CDCl_3$) δ = 7.97 (d, J = 8.4 Hz, 1H), 7.54 (ddd, J = 8.3, 5.8, 2.3 Hz, 1H), 7.47 to 7.40 (m, 2H), 7.17 (d, J = 7.5 Hz, 1H), 7.11 (s, 2H), 6.94 (d, J = 7.5 Hz, 1H). 4.19 (s, 2H), 2.49 (s, 3H), and 2.01 (s, 6H). ^{13}C NMR (100 MHz, $CDCl_3$) δ = 141.13, 137.60, 137.21, 136.58, 132.71, 129.78, 128.08, 127.14, 126.26, 126.00, 124.79, 124.05, 121.19, 109.92, 21.22, 20.48, and 17.83. HRMS; mass/charge ratio (m/z) for $C_{19}H_{19}N$ $[M + H]^+$ calcd.: 262.1590, found 262.1594.

Synthesis of 1-bromo-4-mesitylnaphthalene (4b)

To a solution of 4-mesitylnaphthalen-1-amine (**S2**, 2.09 g, 8 mmol, 1 equiv.), $^nBu_4NBr$ (5.15 g, 16 mmol, and 2 equiv.), and p-TsOH (1.65 g, 9.6 mmol, and 1.2 equiv.) in CH_3CN (100 ml) in a 250-ml round bottom flask was injected 0.88 ml of ^nBuONO (1.0 g, 9.6 mmol, and 1.2 equiv.) with stirring. After 5 min, $CuBr_2$ (90 mg, 0.40 mmol, and 0.05 equiv.) was added, and the resultant mixture was stirred at ambient temperature for 5 hours; the reaction progress was monitored by TLC. After completion of the reaction, the reaction mixture was extracted with CH_2Cl_2. The combined organic layers were dried over Na_2SO_4, and the solvent was removed under reduced pressure. The crude product was purified by silica gel column chromatography using pure hexane to give 1-bromo-4-mesitylnaphthalene (**4b**, 1.84 g, 71%) as a white solid. ^1H NMR (400 MHz, $CDCl_3$) δ = 8.38 (d, J = 8.5 Hz, 1H), 7.91 (d, J = 7.5 Hz, 1H), 7.64 (ddd, J = 8.2, 5.3, 2.5 Hz, 1H), 7.50 to 7.41 (m, 2H), 7.18 (d, J = 7.5 Hz, 1H), 7.08 (s, 2H). 2.46 (s, 3H), and 1.93 (s, 6H). ^{13}C NMR (100 MHz, $CDCl_3$) δ =139.08, 137.23, 136.78, 135.91, 133.33, 132.25, 129.90, 128.23, 127.55, 127.28, 127.20, 126.92, 126.08, 121.82, 21.20, and 20.36. HRMS; m/z for $C_{19}H_{17}Br$ $[M − H]^−$ calcd.: 323.0430 (100%) and 325.0410 (99%). found 323.0435 (100%) and 325.0406 (99%).

Synthesis of 1,3,5,7,9-pentakis(naphthyl)corannulene (5a)

To a solution of $Pd(PPh_3)_4$ (30 mg, 25 μmol, and 0.25 equiv.) in toluene (15 ml) were added 1,3,5,7,9-pentakis(Bpin)corannulene (**3**, 88 mg, 0.1 mmol, and 1 equiv.), 1-bromo-naphthalene (**4a**, 210 mg, 1.0 mmol, and 10 equiv.), $Pd(PPh_3)_4$ (30 mg, 25 μmol, and 0.25 equiv.), and a solution of Cs_2CO_3 (0.98 g, 3.0 mmol, and 30 equiv.) in water (5 ml), and the resultant mixture was stirred at 100°C for 24 hours under nitrogen. After cooling the mixture to room temperature, the reaction was quenched by dilute hydrochloric acid, and the mixture was extracted with CH_2Cl_2 and washed with saturated NaCl solution three times. The combined organic layers were dried over Na_2SO_4,

and the solvent was removed under reduced pressure. The crude product was purified by silica gel column chromatography (eluent: hexane/CS_2 = 1:2) to give 1,3,5,7,9-pentakis(naphthyl)corannulene (**5a**, 39 mg, 44.3%) as a white solid. The ^1H NMR spectrum of **5a** shows broad peaks due to slow rotations of the naphthyl groups at room temperature, and the spectroscopic data matched those reported in the literature (41). ^1H NMR (400 MHz, CD_2Cl_2, 25°C) δ = 8.54 to 7.92 (m, 5H), 7.87 (m, 10H), and 7.59 to 7.26 (m, 25H). ^1H NMR (400 MHz, $C_2D_2Cl_4$, 80°C) δ = 7.92 to 7.86 (m, 10H), 7.57 (s, 5H), and 7.43 to 7.37 (m, 25H). HRMS (FT-ICR); m/z for $C_{70}H_{40}$ $[M + H]^+$ calcd.: 880.3208, found 880.3220.

Synthesis of 1,3,5,7,9-pentakis(4-mesitylnaphthyl) corannulene (5b)

To a solution of $Pd(PPh_3)_4$ (44 mg, 37.5 μmol, and 0.25 equiv.) in toluene (20 ml) were added 1,3,5,7,9-pentakis(Bpin)corannulene (**3**, 132 mg, 0.15 mmol, and 1.0 equiv.), 1-bromo-4-mesitylnaphthalene (**4b**, 490 mg, 1.5 mmol, and 10.0 equiv.), and a solution of Cs_2CO_3 (1.47 g, 4.5 mmol, and 30.0 equiv.) in water (10 ml), and the resultant mixture was stirred at 100°C for 24 hours under nitrogen. After cooling the mixture to room temperature, the reaction was quenched by dilute hydrochloric acid, and the mixture was extracted with CH_2Cl_2. The combined organic layers were washed three times with saturated NaCl solution and dried over Na_2SO_4, and the solvent was removed under reduced pressure. The crude product was purified by silica gel column chromatography (eluent: hexane/CH_2Cl_2 = 1:4) to give 1,3,5,7,9-pentakis(4-mesitylnaphthyl)corannulene (**5b**, 78 mg, 35%) as a light yellow solid. The ^1H NMR of **5b** also shows broad peaks due to slow rotations of the 4-mesitylnaphthyl groups at room temperature. ^1H NMR (500 MHz, CD_2Cl_2, 25°C) δ = 8.58 to 8.07 (m, 5H), 7.78 (m, 5H), 7.65 to 7.54 (m, 5H), 7.50 to 7.24 (m, 20H), 7.01 (s, 10H), 2.42 (s, 15H), 1.92 (s, 15H), and 1.34 (s, 15H). ^1H NMR (400 MHz, $C_2D_2Cl_4$, 80°C) δ = 7.80 to 7.24 (m, 35H), 7.01 (s, 10H), 2.42 (s, 15H), and 1.89 (s, 30H). HRMS (FT-ICR); m/z for $C_{115}H_{90}$ $[M + H]^+$ calcd.: 1471.7121, found 1471.7167.

Synthesis of carboncone (1a)

To a solution of 1,3,5,7,9-pentakis(naphthyl)corannulene (**5a**, 39 mg, 0.044 mmol, and 1.0 equiv.) in dry CH_2Cl_2 (10 ml) was added DDQ (100 mg, 0.44 mmol, and 10.0 equiv.) at 25° or 0°C under nitrogen gas flow. After stirring for about 5 min, trifluoromethanesulfonic acid (0.1 ml) was added to the mixture. The mixture was further stirred for 10 min at 25° or 0°C. The reaction mixture was quenched by adding saturated aqueous $NaHCO_3$. A black precipitate was formed and filtrated, which is almost insoluble in common organic solvents. Therefore, the crude product was only characterized by high-resolution MALDI-TOF MS, which indicates that the product is a mixture. The strongest signal corresponds to the desired carboncone **1a**, and the other signals mainly belong to incomplete ring closure products. HRMS (MALDI-TOF); m/z for $C_{70}H_{20}$ $[M]^{+•}$ calcd.: 860.1559, found 860.1597.

Synthesis of carboncone (1b)

To a solution of 1,3,5,7,9-pentakis(4-mesitylnaphthyl)corannulene (**5b**, 30 mg, 0.02 mmol, and 1 equiv.) in dry CH_2Cl_2 (10 ml) was added DDQ (47 mg, 0.2 mmol, and 10 equiv.) at 25° or 0°C under nitrogen gas flow. After stirring for about 5 min, trifluoromethane-sulfonic acid (0.1 ml) was added to the mixture. The mixture was further stirred for 10 min at 25° or 0°C. The reaction mixture was

quenched by adding saturated aqueous $NaHCO_3$, and then the mixture was extracted with CH_2Cl_2. The combined organic layer was dried over Na_2SO_4, and the solvent was removed under reduced pressure. The crude product was purified by silica gel column chromatography (eluent: hexane/CS_2 = 1: 1) to give the carboncone (**1b**, 14 mg, 46%) as an orange solid. ^1H NMR (500 MHz, CD_2Cl_2) δ = 9.91 (d, J = 9.6 Hz, 1H), 9.84 (s, 1H), 8.72 (d, J = 8.9 Hz, 1H), 7.43 (s, 1H), 7.14 (s, 1H), 2.70 (s, 3H), 2.61 (s, 3H), and 1.54 (s, 3H). ^{13}C NMR (150 MHz, CD_2Cl_2 and CS_2) δ = 192.60, 138.80, 138.71, 137.84, 137.47, 137.28, 136.97, 130.05, 129.02, 128.93, 128.65, 127.98, 127.91, 125.18, 125.08, 124.73, 124.68, 124.57, 123.72, 123.66, 123.53, 21.80, 21.71, and 20.61. HRMS (MALDI-TOF); m/z for $C_{115}H_{70}$ [M]$^{+\bullet}$ calcd.: 1450.5472, found 1450.5450.

SUPPLEMENTARY MATERIALS

Supplementary material for this article is available at http://advances.sciencemag.org/cgi/content/full/5/8/eaaw0982/DC1

Fig. S1. Full synthetic scheme of **1**.
Fig. S2. NMR spectra of **S2**.
Fig. S3. NMR spectra of **4b**.
Fig. S4. ^1H NMR (400 MHz) spectra of **5a**.
Fig. S5. ^1H NMR spectra of **5b**.
Fig. S6. ^{13}C NMR spectra of **5b**.
Fig. S7. MALDI-TOF mass spectra of $C_{70}H_{20}$ (**1a**).
Fig. S8. MALDI-TOF mass spectra of $C_{115}H_{70}$ (**1b**).
Fig. S9. ^1H NMR spectrum of the carboncone (**1b**).
Fig. S10. Theoretical simulations for ^1H NMR spectra of **1b** and the possible heptagon-containing isomer.
Fig. S11. ^{13}C NMR spectrum of the carboncone (**1b**).
Fig. S12. Packing mode of **1b** in the crystal.
Fig. S13. The transition state (TS) structures for cone-to-cone inversion of **1a** and **1b**.
Fig. S14. IRC calculation results of the inversion TS of **1a** and **1b**.
Fig. S15. Structures of compounds **7**, **8**, **9b**, and **10b**.
Fig. S16. Energy barriers for different ring closure steps on **A2** and the relative energies of the intermediate products by a dication pathway.
Fig. S17. Energy barriers for different ring closure steps on **A3** and the relative energies of the intermediate products by a dication pathway.
Fig. S18. Energy barriers for different ring closure steps on **A4** and the relative energies of the intermediate products by a dication pathway.
Fig. S19. Energy barriers for different ring closure steps on **A5** and the relative energies of the intermediate products by a dication pathway.
Fig. S20. Energy barriers for different ring closure steps on **A6** and the relative energies of the intermediate products by a dication pathway.
Fig. S21. Energy barriers for different ring closure steps on **A7** and the relative energies of the intermediate products by a dication pathway.
Fig. S22. Energy barriers for different ring closure steps on **A8** and the relative energies of the intermediate products by a dication pathway.
Fig. S23. Energy barriers for different ring closure steps on **A3'** and the relative energies of the intermediate products by a dication pathway.
Fig. S24. UV-vis absorption spectra of **7** and **8**.
Fig. S25. Molecular orbitals (from HOMO^{-1} to LUMO^{+1}) of carboncone **1a** and **1b** calculated at the B3LYP/6-31G(d,p) level.
Fig. S26. Molecular orbitals (from HOMO^{-1} to LUMO^{+1}) of nanographene **7** calculated at the B3LYP/6-31G(d,p) level.
Fig. S27. Molecular orbitals (from HOMO^{-1} to LUMO^{+1}) of **2** and **8** calculated at the B3LYP/6-31G(d,p) level.
Table S1. Crystallographic data and structure refinement details of **1b**.
Table S2. Cartesian coordinates of optimized species at the B3LYP/6-31G(d,p) level on Gaussian 09.
Table S3. UV-vis absorption of **1a** predicted by TD-DFT calculations at the B3LYP/6-31G(d,p) level.
Table S4. Calculated vibrational frequencies at the B3LYP/6-31G(d,p) level for prominent bands of carboncone **1b** in the IR spectrum (in cm^{-1}).

REFERENCES AND NOTES

1. S. Iijima, T. Ichihashi, Y. Ando, Pentagons, heptagons and negative curvature in graphite microtubule growth. *Nature* **356**, 776–778 (1992).
2. M. Ge, K. Sattler, Observation of fullerene cones. *Chem. Phys. Lett.* **220**, 192–196 (1994).
3. A. Krishnan, E. Dujardin, M. M. J. Treacy, J. Hugdahl, S. Lynum, T. W. Ebbesen, Graphitic cones and the nucleation of curved carbon surfaces. *Nature* **388**, 451–454 (1997).
4. G. Zhang, X. Jiang, E. Wang, Tubular graphite cones. *Science* **300**, 472–474 (2003).
5. P. Ghosh, M. Z. Yusop, S. Satoh, M. Subramanian, A. Hayashi, Y. Hayashi, M. Tanemura, Transparent and flexible field electron emitters based on the conical nanocarbon structures. *J. Am. Chem. Soc.* **132**, 4034–4035 (2010).
6. H. Tanaka, H. Kanoh, M. El-Merraoui, W. A. Steele, M. Yudasaka, S. Iijima, K. Kaneko, Quantum effects on hydrogen adsorption in internal nanospaces of single-wall carbon nanohorns. *J. Phys. Chem. B* **108**, 17457–17465 (2004).
7. S. Iijima, M. Yudasaka, R. Yamada, S. Bandow, K. Suenaga, F. Kokai, K. Takahashi, Nano-aggregates of single-walled graphitic carbon nano-horns. *Chem. Phys. Lett.* **309**, 165–170 (1999).
8. T. W. Odom, J.-L. Huang, P. Kim, C. M. Lieber, Atomic structure and electronic properties of single-walled carbon nanotubes. *Nature* **391**, 62–64 (1998).
9. M. N. Eliseeva, L. T. Scott, Pushing the Ir-catalyzed C–H polyborylation of aromatic compounds to maximum capacity by exploiting reversibility. *J. Am. Chem. Soc.* **134**, 15169–15172 (2012).
10. J. M. Quimby, Ph.D. Dissertation, Boston College, Chestnut Hill, MA (2011).
11. V. M. Tsefrikas, L. T. Scott, Geodesic polyarenes by flash vacuum pyrolysis. *Chem. Rev.* **106**, 4868–4884 (2006).
12. A. Hirsch, M. Brettreich, *Fullerenes: Chemistry and Reactions* (Wiley-VCH, 2005).
13. H. E. Bronstein, N. Choi, L. T. Scott, Practical synthesis of an open geodesic polyarene with a fullerene-type 6:6-double bond at the center: Diindeno[1,2,3,4-*defg*;1',2',3',4'-*mnop*]chrysene. *J. Am. Chem. Soc.* **124**, 8870–8875 (2002).
14. Y.-T. Wu, J. S. Siegel, Aromatic molecular-bowl hydrocarbons: Synthetic derivatives, their structures, and physical properties. *Chem. Rev.* **106**, 4843–4867 (2006).
15. P. von Ragué Schleyer, C. Maerker, A. Dransfeld, H. Jiao, N. J. R. van Eikema Hommes, Nucleus-independent chemical shifts: A simple and efficient aromaticity probe. *J. Am. Chem. Soc.* **118**, 6317–6318 (1996).
16. Chaolumen, M. Murata, A. Wakamiya, Y. Murata, Unsymmetric twofold Scholl cyclization of a 5,11-dinaphthyltetracene: Selective formation of pentagonal and hexagonal rings via dicationic intermediates. *Angew. Chem. Int. Ed.* **56**, 5082–5086 (2017).
17. K. Kawasumi, Q. Zhang, Y. Segawa, L. T. Scott, K. Itami, A grossly warped nanographene and the consequences of multiple odd-membered-ring defects. *Nat. Chem.* **5**, 739–744 (2013).
18. F. Dötz, J. D. Brand, S. Ito, L. Gherghel, K. Müllen, Synthesis of large polycyclic aromatic hydrocarbons: Variation of size and periphery. *J. Am. Chem. Soc.* **122**, 7707–7717 (2000).
19. B. D. Steinberg, E. A. Jackson, A. S. Filatov, A. Wakamiya, M. A. Petrukhina, L. T. Scott, Aromatic π-systems more curved than C_{60}. The complete family of all indenocorannulenes synthesized by iterative microwave-assisted intramolecular arylations. *J. Am. Chem. Soc.* **131**, 10537–10545 (2009).
20. S. Lampart, L. M. Roch, A. K. Dutta, Y. Wang, R. Warshamanage, A. D. Finke, A. Linden, K. K. Baldridge, J. S. Siegel, Pentaindenocorannulene: Properties, assemblies, and C_{60} complex. *Angew. Chem. Int. Ed.* **55**, 14648–14652 (2016).
21. T. J. Seiders, K. K. Baldridge, J. S. Siegel, Synthesis and characterization of the first corannulene cyclophane. *J. Am. Chem. Soc.* **118**, 2754–2755 (1996).
22. O. Allemann, S. Duttwyler, P. Romanato, K. K. Baldridge, J. S. Siegel, Proton-catalyzed, silane-fueled Friedel-Crafts coupling of fluoroarenes. *Science* **332**, 574–577 (2011).
23. A. Sygula, P. W. Rabideau, Non-pyrolytic syntheses of buckybowls: Corannulene, cyclopentacorannulene, and a semibuckminsterfullerene. *J. Am. Chem. Soc.* **121**, 7800–7803 (1999).
24. K. Y. Amsharov, M. A. Kabdulov, M. Jansen, Facile bucky-bowl synthesis by regiospecific cove-region closure by HF elimination. *Angew. Chem. Int. Ed.* **51**, 4594–4597 (2012).
25. K. Y. Cheung, X. Xu, Q. Miao, Aromatic saddles containing two heptagons. *J. Am. Chem. Soc.* **137**, 3910–3914 (2015).
26. H. Omachi, Y. Segawa, K. Itami, Synthesis of cycloparaphenylenes and related carbon nanorings: A step toward the controlled synthesis of carbon nanotubes. *Acc. Chem. Res.* **45**, 1378–1389 (2012).
27. L. T. Scott, E. A. Jackson, Q. Zhang, B. D. Steinberg, M. Bancu, B. Li, A short, rigid, structurally pure carbon nanotube by stepwise chemical synthesis. *J. Am. Chem. Soc.* **134**, 107–110 (2012).
28. G. Povie, Y. Segawa, T. Nishihara, Y. Miyauchi, K. Itami, Synthesis of a carbon nanobelt. *Science* **356**, 172–175 (2017).
29. E. H. Fort, L. T. Scott, Carbon nanotubes from short hydrocarbon templates. Energy analysis of the Diels–Alder cycloaddition/rearomatization growth strategy. *J. Mater. Chem.* **21**, 1373–1381 (2011).
30. H.-B. Li, A. J. Page, S. Irle, K. Morokuma, Single-walled carbon nanotube growth from chiral carbon nanorings: Prediction of chirality and diameter influence on growth rates. *J. Am. Chem. Soc.* **134**, 15887–15896 (2012).
31. X. Yu, J. Zhang, W. M. Choi, J.-Y. Choi, J. M. Kim, L. Gan, Z. Liu, Cap formation engineering: From opened C_{60} to single-walled carbon nanotubes. *Nano Lett.* **10**, 3343–3349 (2010).

32. H. Omachi, T. Nakayama, E. Takahashi, Y. Segawa, K. Itami, Initiation of carbon nanotube growth by well-defined carbon nanorings. *Nat. Chem.* **5**, 572–576 (2013).

33. B. Liu, J. Liu, H.-B. Li, R. Bhola, E. A. Jackson, L. T. Scott, A. Page, S. Irle, K. Morokuma, C. Zhou, Nearly exclusive growth of small diameter semiconducting single-wall carbon nanotubes from organic chemistry synthetic end-cap molecules. *Nano Lett.* **15**, 586–595 (2015).

34. J. R. Sanchez-Valencia, T. Dienel, O. Gröning, I. Shorubalko, A. Mueller, M. Jansen, K. Amsharov, P. Ruffieux, R. Fasel, Controlled synthesis of single-chirality carbon nanotubes. *Nature* **512**, 61–64 (2014).

35. A. M. Butterfield, B. Gilomen, J. S. Siegel, Kilogram-scale production of corannulene. *Org. Process Res. Dev.* **16**, 664–676 (2012).

36. G. M. Sheldrick, Crystal structure refinement with *SHELXL*. *Acta Cryst.* **C71**, 3–8 (2015).

37. O. V. Dolomanov, L. J. Bourhis, R. J. Gildea, J. A. K. Howard, H. Puschmann, *OLEX2*: A complete structure solution, refinement and analysis program. *J. Appl. Cryst.* **42**, 339–341 (2009).

38. M. J. Frisch, G. W. Trucks, H. B. Schlegel, G. E. Scuseria, M. A. Robb, J. R. Cheeseman, G. Scalmani, V. Barone, B. Mennucci, G. A. Petersson, H. Nakatsuji, M. Caricato, X. Li, H. P. Hratchian, A. F. Izmaylov, J. Bloino, G. Zheng, J. L. Sonnenberg, M. Hada, M. Ehara, K. Toyota, R. Fukuda, J. Hasegawa, M. Ishida, T. Nakajima, Y. Honda, O. Kitao, H. Nakai, T. Vreven, J. A. Montgomery Jr., J. E. Peralta, F. Ogliaro, M. Bearpark, J. J. Heyd, E. Brothers, K. N. Kudin, V. N. Staroverov, R. Kobayashi, J. Normand, K. Raghavachari, A. Rendell, J. C. Burant, S. S. Iyengar, J. Tomasi, M. Cossi, N. Rega, J. M. Millam, M. Klene, J. E. Knox, J. B. Cross, V. Bakken, C. Adamo, J. Jaramillo, R. Gomperts, R. E. Stratmann, O. Yazyev, A. J. Austin, R. Cammi, C. Pomelli, J. W. Ochterski, R. L. Martin, K. Morokuma, V. G. Zakrzewski, G. A. Voth, P. Salvador, J. J. Dannenberg, S. Dapprich, A. D. Daniels, Ö. Farkas, J. B. Foresman, J. V. Ortiz, J. Cioslowski, D. J. Fox, Gaussian 09, revision D.01 (Gaussian Inc., 2016).

39. T. C. Wu, M. K. Chen, Y. W. Lee, M. Y. Kuo, Y.-T. Wu, Bowl-shaped fragments of C$_{70}$ or higher fullerenes: Synthesis, structural analysis, and inversion dynamics. *Angew. Chem. Int. Ed.* **52**, 1289–1293 (2013).

40. T. E. Barder, S. D. Walker, J. R. Martinelli, S. L. Buchwald, New catalysts for Suzuki-Miyaura coupling processes: Scope and studies of the effect of ligand structure. *J. Am. Chem. Soc.* **127**, 4685–4696 (2005).

41. G. H. Grube, E. L. Elliott, R. J. Steffens, C. S. Jones, K. K. Baldridge, J. S. Siegel, Synthesis and properties of *sym*-pentasubstituted derivatives of corannulene. *Org. Lett.* **5**, 713–716 (2003).

Science Advances

Rational synthesis of an atomically precise carboncone under mild conditions

Zheng-Zhong Zhu, Zuo-Chang Chen, Yang-Rong Yao, Cun-Hao Cui, Shu-Hui Li, Xin-Jing Zhao, Qianyan Zhang, Han-Rui Tian, Piao-Yang Xu, Fang-Fang Xie, Xiao-Ming Xie, Yuan-Zhi Tan, Shun-Liu Deng, Jennifer M. Quimby, Lawrence T. Scott, Su-Yuan Xie, Rong-Bin Huang and Lan-Sun Zheng

ARTICLE TOOLS	http://advances.sciencemag.org/content/5/8/eaaw0982
SUPPLEMENTARY MATERIALS	http://advances.sciencemag.org/content/suppl/2019/08/19/5.8.eaaw0982.DC1
REFERENCES	This article cites 38 articles, 3 of which you can access for free http://advances.sciencemag.org/content/5/8/eaaw0982#BIBL
PERMISSIONS	http://www.sciencemag.org/help/reprints-and-permissions

Use of this article is subject to the Terms of Service